MRI Virtual Biopsy and Treatment of Brain Metastatic Tumors with Targeted Nanobioconjugates: Nanoclinic in the Brain

Rameshwar Patil,[†] Alexander V. Ljubimov,[†,⊥,#,▽] Pallavi R. Gangalum,[†] Hui Ding,[†] Jose Portilla-Arias,[†] Shawn Wagner,[‡] Satoshi Inoue,[†,¶] Bindu Konda,[†] Arthur Rekechenetskiy,[†] Alexandra Chesnokova,[†] Janet L. Markman,[†] Vladimir A. Ljubimov,[§] Debiao Li,[‡] Ravi S. Prasad,[∥] Keith L. Black,[†,⊥,#,▽,□] Eggehard Holler,[†,⊥,#,▽,□] and Julia Y. Ljubimova*[,†,⊥,#,▽,□]

[†]Department of Neurosurgery, [‡]Biomedical Imaging Research Institute, Department of Biomedical Sciences, [∥]Department of Imaging, [⊥]Samuel Oschin Comprehensive Cancer Center, and [▽]Department of Biomedical Sciences, Cedars-Sinai Medical Center, Los Angeles, California, United States, [§]Keck School of Medicine, University of Southern California, Los Angeles, California, United States, and [#]Arrogene Inc., Los Angeles, California, United States. [□]K. L. Black, E. Holler, and J. Y. Ljubimova contributed equally to this paper. [¶]Present address: Department of Advanced Trauma Surgery, Saga-city, Saga, Japan.

ABSTRACT Differential diagnosis of brain magnetic resonance imaging (MRI) enhancement(s) remains a significant problem, which may be difficult to resolve without biopsy, which can be often dangerous or even impossible. Such MRI enhancement(s) can result from metastasis of primary tumors such as lung or breast, radiation necrosis, infections, or a new primary brain tumor (glioma, meningioma). Neurological symptoms are often the same on initial presentation. To develop a more precise noninvasive MRI diagnostic method, we have engineered a new class of poly(β-L-malic acid) polymeric nanoimaging agents (NIAs). The NIAs carrying attached MRI tracer are able to pass through the blood–brain barrier (BBB) and specifically target cancer cells for efficient imaging. A qualitative/quantitative "MRI virtual biopsy" method is based on a nanoconjugate carrying MRI contrast agent gadolinium-DOTA and antibodies recognizing tumor-specific markers and extravasating through the BBB. In newly developed double tumor xenogeneic mouse models of brain metastasis this noninvasive method allowed differential diagnosis of HER2- and EGFR-expressing brain tumors. After MRI diagnosis, breast and lung cancer brain metastases were successfully treated with similar tumor-targeted nanoconjugates carrying molecular inhibitors of EGFR or HER2 instead of imaging contrast agent. The treatment resulted in a significant increase in animal survival and markedly reduced immunostaining for several cancer stem cell markers. Novel NIAs could be useful for brain diagnostic MRI in the clinic without currently performed brain biopsies. This technology shows promise for differential MRI diagnosis and treatment of brain metastases and other pathologies when biopsies are difficult to perform.

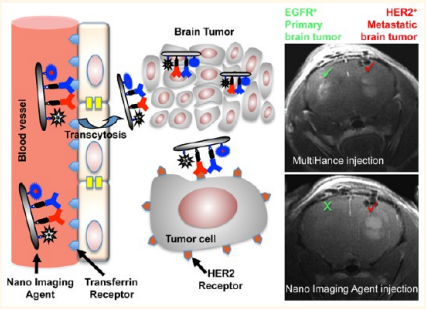

KEYWORDS: nanoconjugate · brain metastasis · MRI · nanomedicine · blood–brain barrier · tumor treatment · tumor targeting

A significant clinical problem in brain metastasis (BM) management is limitation of diagnostic imaging for identifying the etiology of contrast-enhancing lesions seen on magnetic resonance imaging (MRI), in order to plan the treatment strategy. Contrast enhancement in the brain of a cancer patient could result from primary tumor metastasis, infection in an immunocompromised patient after chemotherapy, or a primary brain tumor (Figure 1). In a patient treated for BM or primary central nervous system (CNS) neoplasm, post-treatment radiation necrosis can mimic tumor recurrence. Neurological symptoms are often the same for a recurrence and brain infection on initial presentation. Without a history of a cancer, a solitary enhancing lesion in the brain carries a broad differential including metastatic disease or primary CNS tumor. Primary brain tumors are relatively rare, but BM is a significant clinical problem. Lung and breast are the top tumors associated with BM, which accounts for 20–30% of cancer deaths annually.[1−6] BM is present in up to 40% of metastatic lung cancers and 25% of metastatic breast cancers, with autopsy revealing about twice as many cases.[7,8] Non-small-cell lung cancer shows higher BM incidence

* Address correspondence to ljubimovaj@cshs.org.

Received for review March 27, 2015 and accepted April 23, 2015.

Published online April 23, 2015
10.1021/acsnano.5b01872

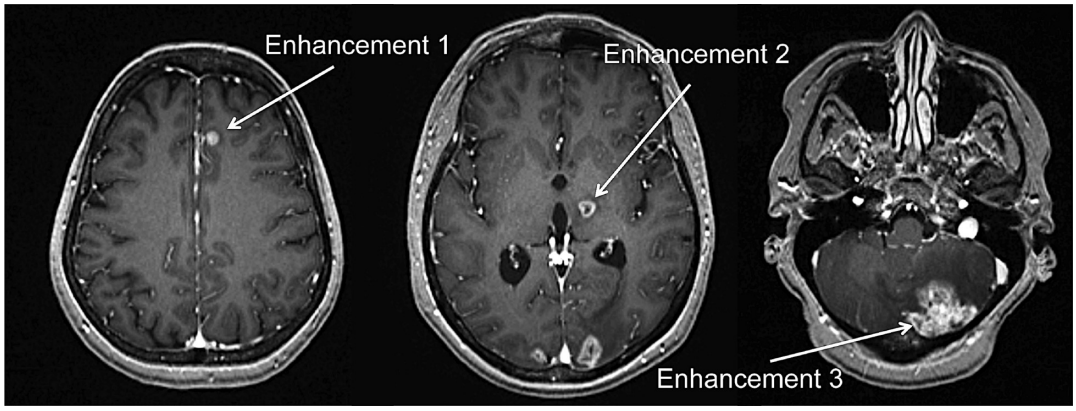

Figure 1. MRI enhancement of multiple brain lesions of a 48 y.o. female with HER2/*neu* positive breast carcinoma with brain metastasis. MRI scan with multiple enhancements in the brain can result from metastasis of primary tumors (*e.g.*, breast), radiation necrosis, infections, or a new primary brain tumor.

followed by small-cell lung cancer.[8] A significant proportion of breast cancers overexpressing epidermal growth factor receptor-2 (HER2/*neu*) and triple-negative breast cancers (TNBC) lacking estrogen, progesterone, and HER2 receptors, but overexpressing epidermal growth factor receptor-1 (EGFR), also develop BM with poor survival outcome.[9−12] Progress in primary cancer treatment has led to an increase in patients' longevity but has also increased the chance of residual cells metastasizing, in particular to the brain.[13,14] The median survival of patients with BM ranges from 3 to 6 months.

Clinically used therapeutic monoclonal antibodies (mAbs), *e.g.*, trastuzumab (to HER2) for breast and ovarian cancer, cetuximab (to EGFR) for lung and breast cancer, and rituximab (to CD20) for lymphoma, are effective for primary tumor treatment but cannot penetrate the endothelial blood−brain barrier (BBB)[15] to reach brain tumors and hence fail to treat BM.[13,16] Nevertheless, these antibodies can well be used for brain drug delivery[17] when they are part of nanovehicles[18,19] capable of efficiently crossing the BBB.[20,21]

Verification of brain MRI enhancements from primary or secondary (metastatic) brain tumors remains problematic.[7] MultiHance is a gadolinium (Gd)-based MRI contrast agent routinely used in the clinic and is highly effective in detecting a variety of tumors. However, it cannot discriminate brain MRI enhancement due to BM from other lesions with different etiology or from *de novo* primary brain tumors.

Due to these shortcomings in the diagnostic MRI for brain tumors and BMs, there is a significant need for brain tumor-targeted agents suitable for MRI use and capable of differentiating malignant MRI brain enhancements. To circumvent this problem, we have engineered a new class of MRI nanoimaging agents (NIAs) based on the poly(β-L-malic acid) (PMLA) delivery platform. Besides its biodegradability, lack of toxicity, and immunogenicity,[22] it offers high versatility for on-demand covalent conjugation of various moieties including proteins, chemotherapeutic agents, nucleic acids, and imaging agents.[17,23,24] Here, we present a noninvasive tumor-specific imaging approach, "MRI virtual biopsy", by engineering a new NIA on a PMLA scaffold containing Gd-DOTA as a contrast agent for differential diagnosis of brain tumors. Gd-DOTA is the safest contrast agent among other Gd-chelates due to its extremely high stability.[25] The strategy is that after noninvasive MRI diagnosis recognizing the brain lesion on the basis of its molecular signatures, the tumor (primary cancer or BM) is suppressed by tumor-specific molecular inhibitor(s) delivered by a PMLA-based nanoconjugate, which is structurally similar to the used NIA. This technology was developed to differentiate and treat metastatic brain cancer in new murine models using their tumor-specific molecular markers. It could be expanded beyond verification of brain tumor type by MRI to the differentiation of inflammation, infection, and other brain pathological conditions without neurosurgical intervention.

RESULTS AND DISCUSSION

Synthesis of Nanoimaging Agents and Nanodrugs. MRI enhancement(s) diagnoses often require invasive histological tissue biopsy verification, which may be difficult to perform for brain lesions. To develop a more precise noninvasive MRI diagnostic method, we have engineered a new class of poly(β-L-malic acid) polymeric nanoimaging agents for identification of different tumors based on specific molecular markers. To accomplish this task, we combined the expertise of magnetic resonance physicists, synthetic chemists, molecular biologists, cancer researchers, clinical radiologists, and neurosurgeons.

Two types of PMLA-based nanoconjugates for either brain tumor imaging (Figure 2) or treatment (Figure S1) containing various functional moieties and payloads were separately prepared from intermediates, Preconjugate-1 and Preconjugate-2, respectively. Preconjugate-1 of the NIA (Figure 2b) was synthesized by activation of PMLA pendant carboxyl groups and sequential addition of gadolinium-DOTA-NH_2 (MRI

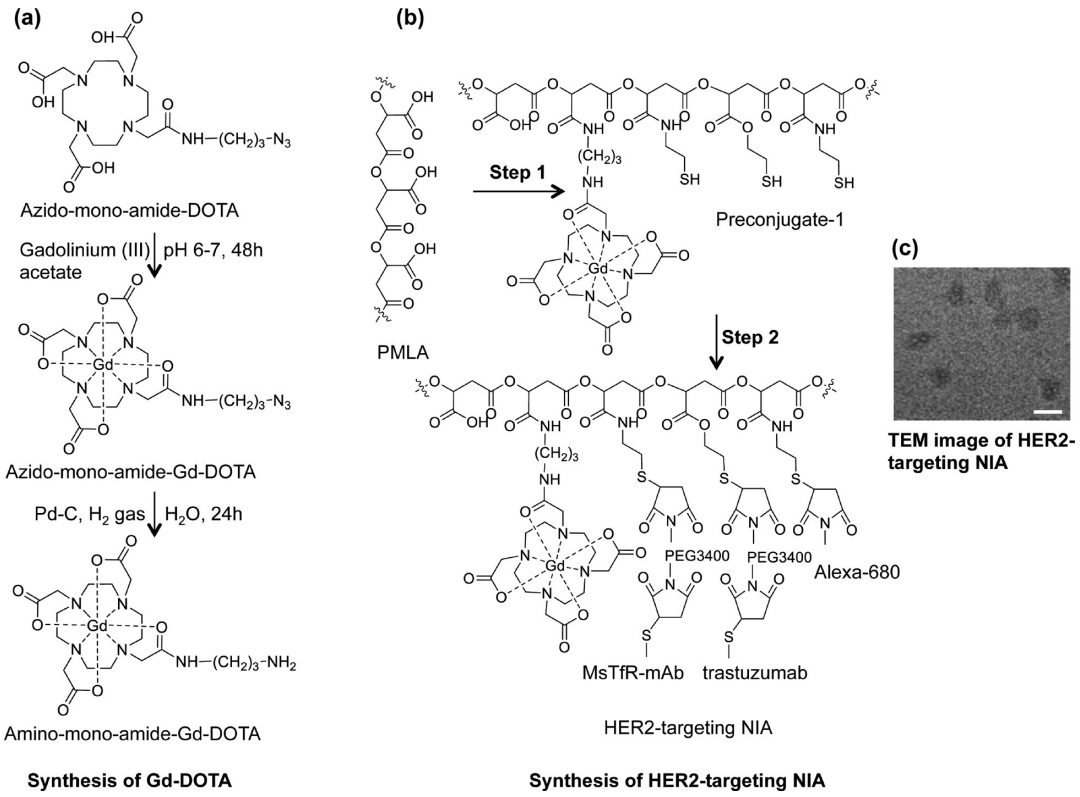

Figure 2. Synthesis of nanoimaging agent for MRI and fluorescent imaging (HER-2 targeting NIA is shown). (a) Synthesis of Gd-DOTA amine. Metal complex was prepared by reacting azido-monoamide-DOTA with 1.1 molar excess of gadolinium(III) acetate while maintaining the pH between 6 and 7. Azido-monoamide-Gd-DOTA was dissolved in water (25 mg/mL), and hydrogenolysis was carried out by hydrogen gas in the presence of 10% (w/w) Pd−C (palladium on carbon). The product (amino-monoamide-Gd-DOTA) was used for further reactions without any additional purification. (b) *Step 1*: Attachment of Gd-DOTA and 2-mercapto-1-ethylamine (MEA) through amide linkage after *N*-hydroxysuccinimide (NHS) activation of PMLA's pendant carboxylates. The product (Preconjugate-1) was purified by size exclusion chromatography and obtained as a white floppy solid after lyophilization. Preconjugate-1 is stable at −20 °C for months without measurable loss in chemical or physicochemical reactivity. *Step 2:* Maleimide-functionalized mAbs and Alexa-680 were conjugated by a stable thioether bond. Trastuzumab was chosen for HER2 targeting (as shown), and cetuximab was chosen for EGFR targeting (not shown here). Anti-mouse TfR (MsTfR) mAb is used for tumor endothelial binding and transcytosis. Finally excess thiol groups masked using PDP and products were purified by PD-10 columns. (c) TEM image of HER2-targeting NIA. Scale bar = 25 nm.

contrast agent Gd-DOTA, Figure 2a) and 2-mercapto-1-ethylamine (MEA). Likewise, Preconjugate-2 (Figure S1) was synthesized by sequential addition of mPEG5000-NH_2 (mPEG), H_2N-Leu-ethyl ester (LOEt), and MEA. In the second part of the synthesis, sulfhydryl groups (−SH) were conjugated with chemically activated mAbs for tumor targeting, morpholino antisense oligonucleotides (AONs) for inhibition of HER2/*neu* (HER2-AON) or EGFR (EGFR-AON) mRNA, and an optional imaging agent Alexa Fluor 680 (Alexa-680). Maleimidated mAbs and maleimidated Alexa-680 were attached to preconjugates as thioethers. Flow cytometry experiments using cultured tumor cells confirmed that the conjugated mAbs cetuximab and trastuzumab strongly bound to EGFR and HER2 receptors, respectively (Figure S2). NIAs targeting $HER2^+$ tumors with mAb trastuzumab to HER2 (Figure 2) had diameters in the range 15−18 nm, measured by transmission electron microscopy (TEM, Figure 2c). Nanoconjugate composition and hydrodynamic diameter/zeta potential are summarized in Table 1. For detailed synthesis and purification see Material and Methods and the Supporting Information.

Physicochemical Characterization of Nanodrugs. Nanoconjugates were highly purified, as validated by sec-HPLC and dynamic light scattering (DLS, number distribution), and highly soluble in aqueous solution without forming precipitates/aggregates. The composition of functional moieties was confirmed by chemical analysis and corresponds by ±5% to the designed stoichiometries. Hydrodynamic diameters and zeta potentials had characteristic values in the range of 8 to 17 nm and −2 to −17 mV, respectively (Table 1). Free PMLA, Preconjugate-1, and Preconjugate-2 had relatively small hydrodynamic diameters of 6.6 ± 0.1, 8.8 ± 0.7, and 8.1 ± 0.5 nm, respectively. Due to free carboxylates, unmodified PMLA has a high negative zeta potential value of −22.9 mV (±1.7). After chemical loading of intermediates and drugs, the zeta potential of nanodrugs significantly changed toward neutral (−2.5 to −4 mV), favoring conditions optimal for cellular uptake. MRI contrast agents

TABLE 1. Summary of Nanoconjugates, their Abbreviations, and Physicochemical Characterization

imaging and treatment agents	abbreviations	hydrodynamic diameter (nm)[a]	zeta potential (mV)[b]
poly(β-L-malic acid)	PMLA	6.6 ($\pm$0.1)	−22.9 ($\pm$1.7)
P/MEA(4%)/Gd-DOTA(10−12%)[c]	Preconjugate-1	8.8 ($\pm$0.7)	−16.8 ($\pm$1.8)
P/cetuximab(0.12%)/MsTfR-mAb(0.12%)/Alexa-680(1%)/Gd-DOTA(10−12%)	P/Gd-DOTA/cetuximab/MsTfR-mAb/Alexa-680	16.0 ($\pm$1.5)	−8.7 ($\pm$1.2)
P/trastuzumab(0.12%)/MsTfR-mAb(0.12%)/Alexa-680(1%)/Gd-DOTA(10−12%)	P/Gd-DOTA/trastuzumab/MsTfR-mAb/Alexa-680	16.3 ($\pm$1.6)	−6.9 ($\pm$1.1)
P/mPEG(5%)/LOEt(40%)/MEA(4−6%)	Preconjugate-2	8.1 ($\pm$0.5)	−8.5 ($\pm$1.2)
P/mPEG(5%)/LOEt(40%)/HuTfR-mAb(0.2%)/MsTfR-mAb(0.2%)/EGFR-AON(2−4%)	P/Hu/MsTfR-mAb/EGFR-AON	15.7 ($\pm$2.0)	−2.6 ($\pm$0.8)
P/mPEG(5%)/LOEt(40%)/trastuzumab(0.2%)/MsTfR-mAb(0.2%)/HER2-AON(3−4%)	P/trastuzumab/MsTfR-mAb/HER2-AON	15.7 ($\pm$2.0)	−4.1 ($\pm$0.8)

[a] Hydrodynamic diameter by number distribution at 25 °C measured in PBS at a concentration of 2 mg/mL, calculated from DLS data by the Malvern Zetasizer software (Malvern Instruments, Malvern, UK), which assumes spherical shapes of particles. [b] Zeta potential at 25 °C in an aqueous solution of 10 mM NaCl at 150 mV. [c] Composition of nanoconjugates; percentage refers to total number (100%) of pendant carboxyl groups in unsubstituted PMLA.

P/Gd-DOTA/cetuximab/MsTfR-mAb/Alexa-680 and P/Gd-DOTA/trastuzumab/MsTfR-mAb/Alexa-680 each contained approximately 66 mol of Gd per moles of reagent on average. Zeta potentials were in the range of −9 to −7 mV. In MRI measurements, T1 relaxivities at 3.0 T were 2.0 (mM Gd)$^{-1}$ s^{-1} for MultiHance and 10.0 (mM Gd)$^{-1}$ s^{-1} or 654 (mM reagent)$^{-1}$ s^{-1} for P/Gd-DOTA/cetuximab/MsTfR-mAb/Alexa-680. At the higher field strength of 9.4 T, the relaxivities were 2.0 (mM Gd)$^{-1}$ s^{-1} for MultiHance and 6.0 (mM Gd)$^{-1}$ s^{-1} or 392 (mM reagent)$^{-1}$ s^{-1} for P/Gd-DOTA/cetuximab/MsTfR-mAb/Alexa-680 and P/Gd-DOTA/trastuzumab/MsTfR-mAb/Alexa-680.

Nanoconjugates for Dual Modality Diagnostic Imaging of EGFR- and HER2-Positive Tumor Metastases in the Brain. Mice bearing intracranial EGFR-overexpressing TNBC (MDA-MB-468) as a model of BM were injected intravenously (iv) with the clinical contrast agent MultiHance (0.1 mmol Gd/kg). T1-scans showed peak contrast at 20 min, followed by a fast decline at 60 min and return to baseline before 180 min (Figure 2b, left column). The next day, the same animals were injected iv with EGFR-targeting NIA (P/Gd-DOTA/cetuximab/MsTfR-mAb/Alexa-680, at 0.1 mmol Gd/kg), and MRI scans were recorded in the same time interval (Figure 3a, middle column). The contrast enhancement was retained much longer for the EGFR-targeting NIA than for MultiHance (Figure 3a). To establish whether the signal prolongation was target-specific, HER2-targeting NIA (P/Gd-DOTA/trastuzumab/MsTfR-mAb/Alexa-680, also at 0.1 mmol Gd/kg) was iv injected into animals with the EGFR$^+$ TNBC in the brain. Contrast was enhanced until 60 min, however, significantly less than previously seen for the EGFR-targeted NIA (Figure 3a, right column), and the decay was significantly faster. Thus, specific EGFR targeting maintained a significantly higher contrast ($p < 0.01$) than nonspecific contrast agents during 60 to 180 min after injection (Figure 3b). This suggested that the contrast intensity seen for P/Gd-DOTA/cetuximab/MsTfR-mAb/Alexa-680 reflected specific binding of the NIA to EGFR receptors on TNBC cells. The MRI results were validated by whole-body fluorescent imaging, taking advantage of the attached fluorescent dye Alexa-680. Brain collected from mice 8 h after systemic delivery showed intensive fluorescence for the tumor-targeting NIA P/Gd-DOTA/cetuximab/MsTfR-mAb/Alexa-680 when compared with non-targeted NIA P/Gd-DOTA/trastuzumab/MsTfR-mAb/Alexa-680. Consistent with the observed tumor specificity, cryosections indicated significant amounts of the targeted contrast agent (red) in the tumor cells close to blood vessels, whereas a very small amount of nontargeted NIA was seen only in blood vessels (Figure 3c).

EGFR and HER2 Overexpressing Double Brain Tumor Model Validated by Differential MRI Diagnosis and by Tumor Marker Staining. The novel MRI methodology was used to identify EGFR-overexpressing human glioblastoma (GBM) derived from cell line U87MG growing in one brain hemisphere and a human HER2$^+$ BT-474 breast tumor in the contralateral hemisphere. An imaging study was performed 3−4 weeks post tumor inoculation when both tumors were synchronized in growth and had established their own vascular system. The EGFR$^+$ GBM in the left hemisphere displayed high and prolonged MRI signal intensity (Figure 4a and c) after targeted NIA P/Gd-DOTA/cetuximab/MsTfR-mAb/Alexa-680 at 0.1 mmol Gd/kg (Figure 4b) had been iv administered. The HER2$^+$ breast tumor signal in the right hemisphere had significantly lower intensity and showed a faster decay (Figure 4c). The relative difference in intensity was calculated using several regions of interest (ROI), as shown in (Figure S3). The diagnosis made by the "MRI virtual biopsy" method was correct, as demonstrated by tissue immunostaining for EGFR and HER2 (Figure 4d). Thus, it was possible to identify an EGFR$^+$ GBM in the left hemisphere in the presence of HER2$^+$ metastatic breast tumor in the right hemisphere within the same mouse brain.

In a complementary approach, we demonstrated an identification of HER2$^+$ metastatic breast cancer in the right hemisphere in the presence of EGFR$^+$ GBM in the left hemisphere (Figure 5a). Twenty minutes after iv injection of the targeted NIA P/Gd-DOTA/trastuzumab/MsTfR-mAb/Alexa-680 at 0.1 mmol Gd/kg (Figure 5b),

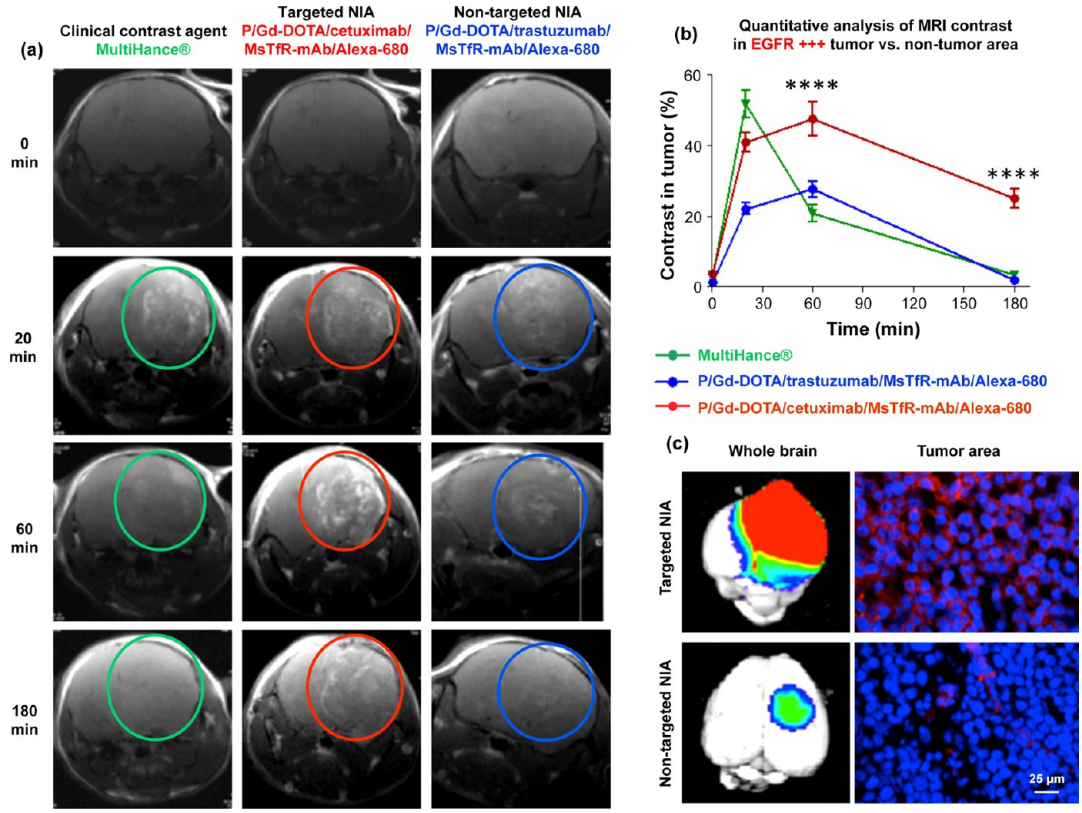

Figure 3. Imaging of TNBC metastasis by dynamic contrast MRI, fluorescence imaging of excised brain after animal euthanasia, and fluorescence microscopy of histological sections. (a) MRI scans of mouse brains with MDA-MB-468 tumors (EGFR+) after iv injection of contrast agents MultiHance, P/Gd-DOTA/cetuximab/MsTfR-mAb/Alexa-680 (targeted NIA), and P/Gd-DOTA/trastuzumab/MsTfR/Alexa-680 (nontargeted NIA). Bright contrast was observed with targeted NIA (red circles) and was maintained for a prolonged time in comparison with MultiHance (green circles) or nontargeting NIA (blue circles). (b) Image quantification based on intensities of regions of interest (ROI; see Figure S3). Intensity from ROIs was calculated using Leica MM AF 1.6 software and normalized at each time point *vs* ROI intensity outside the tumor area. Targeted NIA showed significant difference in MRI contrast intensity *vs* MultiHance or nontargeted NIA at 60 min to 3 h time points (**$p < 0.0001$). (c) Fluorescence of drug targeted into tumor area was used for brain imaging by Xenogen IVIS 200 (left) and for tumor section fluorescence microscopy (right). By microscopy of brain sections, targeted agent (red) was localized in tumor cells around the nuclei (DAPI counterstain, blue). Nontargeted agent was detected only in blood vessels in very small amount.**

an enhancement was detected in both tumors. However, in agreement with our findings, the tumor in the right hemisphere showed high and prolonged intensity, while the tumor intensity in the left hemisphere was significantly lower starting from 1 h and fast decaying (Figure 5c). At earlier times, the difference between receptor-negative and -positive tumor was lower in the case of HER2 than in the case of EGFR. Apparently, the signal in $EGFR^+$ U87MG detected for the first hour by HER2-targeting NIA could be due to the enhanced permeability and retention effect for tumor vasculature, possibly increased in this case by high vascularity and large $EGFR^+$ tumor size. However, this signal was also washed away sooner than the specific one in HER2+ positive tumor, and after 1 h MRI imaging allowed reliable distinction of lesions based on tumor molecular signatures. In all cases examined, the contrast enhancement was no longer detectable at 24 h after injection. The same result was obtained by using MRI contrast dual modality reagents in the fluorescence-imaging mode, which exceeds the MRI mode in detection sensitivity. This finding of relatively rapid washing out of tumor-specific contrast agents would allow repeated MRI imaging of the same brain tumor after 24 h intervals. Immunohistochemical analysis clearly supported the MRI diagnosis that the tumor responding to NIA P/Gd-DOTA/trastuzumab/MsTfR-mAb/Alexa-680 was indeed $HER2^+$ breast cancer BM (Figure 5d). Therefore, both MRI contrast agents were able to identify the type of targeted tumor in the presence of a nontargeted type of tumor. To our knowledge, there is no other known method to provide this analysis in living animals and especially in the brain. Such noninvasive diagnostics could be highly useful to plan an effective treatment strategy in a clinical setting.

Antisense Oligonucleotide Drug Delivery through the BBB into the Cells of Metastatic Brain Tumors *in Vivo*. To demonstrate the ability of a nanodrug to pass through biological barriers such as the BBB, nanodrugs were labeled with two different fluorophores. A PMLA backbone

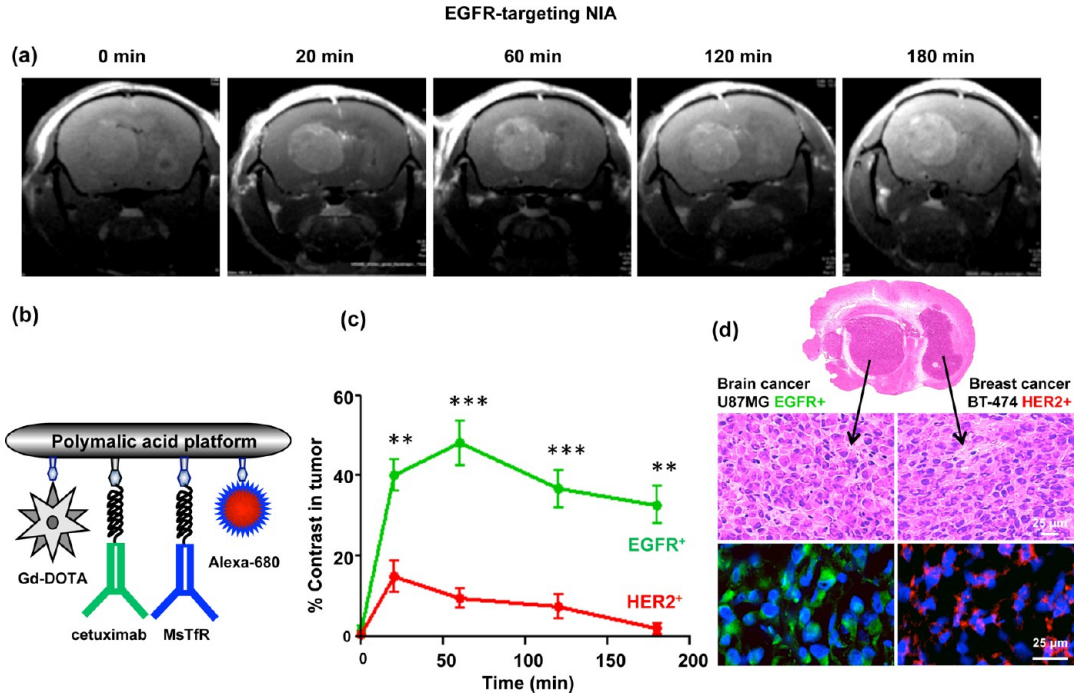

Figure 4. Detection of EGFR$^+$ GBM in the presence of HER2$^+$ metastatic tumor (double tumor model) using EGFR-targeting NIA. (A) MRI brain scans of mice with double tumors, a GBM (U87MG, EGFR$^+$) in the left hemisphere and metastatic breast cancer (BT-474, HER2$^+$) in the right hemisphere after iv injection of targeted NIA (P/Gd-DOTA/cetuximab/MsTfR-mAb/Alexa-680). (b) Schematic presentation of dual modality (MRI contrast and optical) imaging agent. Gd-DOTA is attached *via* amide linkage. Maleimide-functionalized mAbs (cetuximab and MsTfR) and optical agent (Alexa-680) are attached by a stable thioether bond. Cetuximab is used for active tumor targeting, and MsTfR mAb is used for endothelial targeting and transcytosis. (c) Quantitative analysis of MRI contrast in tumors. High contrast in the targeted GBM tumor was maintained beyond 3 h, whereas contrast in the nontargeted HER2$^+$ tumor was low and approached the baseline after 2−3 h ($p < 0.01$; ***$p < 0.001$). (d) Confirmation of the MRI diagnosis by immunohistochemical analysis. Brain sections indicated the presence of two tumors by H&E staining. Brain areas identified by MRI as GBM stained positively with anti-EGFR (green) antibodies, and areas not identified by MRI as EGFR$^+$ stained with anti-HER2 (red) antibodies.**

was labeled with Alexa-680 (pseudogreen), and AONs were labeled with Lissamine (red). Anti-von Willebrand factor (vWF) antibody was used to identify blood vessels (pseudomagenta). We used anti-mouse TfR mAb as a vehicle to transcytose nanodrugs through the mouse endothelial system and either trastuzumab or anti-human TfR mAb as tumor-targeting agent. Microscopic analysis of brain sections showed abundant fluorescence for both Alexa-680 (green arrows) and Lissamine (red arrows) only in the tumor area for three different tumors. Both nanodrugs were able to extravagate through the BBB, and both PMLA and AONs showed distinct colocalization (yellow, white arrows) in the tumor cells in all three metastatic xenograft models, with virtually no signal in the adjacent healthy brain (Figure 6). Tumor blood vessels were void of any noticeable fluorescence for either the AONs or the PMLA backbone, demonstrating the specificity of nanodrug to cancer cells. To validate these results, we used a nanodrug with nonspecific IgG instead of targeting antibody (P/IgG/AON-Lissamine/Alexa-680) in two metastatic tumor models (A-549 and BT-474). No drug was detected in either tumor or healthy brain tissue (Figure S4). The data suggest that nanoconjugates efficiently crossed the BBB, became internalized by the tumor cells, and delivered AONs selectively to malignant cells. The probable mechanism of nanodrug action is schematically shown in (Figure 7).

Enhanced Survival of Mice Bearing Metastatic Brain Tumors Following Inhibition of Specific Pathways with Nanodrugs. Mice with intracranially inoculated BT-474 HER2$^+$ breast cancer cells were treated iv with either P/trastuzumab/MsTfR-mAb/HER2-AON nanodrug or PBS (control) (Figure 8a). Free trastuzumab is inefficient for the treatment of metastatic brain tumors due to its inability to pass through the BBB.[26−28] However, when trastuzumab was covalently conjugated to PMLA together with anti-mouse TfR antibodies for delivery across the BBB, it reached tumor cells, playing a dual role as specific targeting antibody to HER2$^+$ cells and as inhibitor of activation of existing HER2 receptors.[24] Anti-HER2 AONs were used to additionally inhibit the synthesis of new HER2 (Figure 8d and g). The survival of nanodrug-treated mice was increased by 57% *vs* PBS-treated animals (median survival 49.5 days for PBS *vs* 77.5 days for the nanodrug, $p < 0.005$) (Figure 8a). In the brain metastatic model of A-549 EGFR$^+$ lung cancer (Figure 8b), we observed a 66% improvement in survival when treated with P/Hu/MsTfR-mAb/EGFR-AON

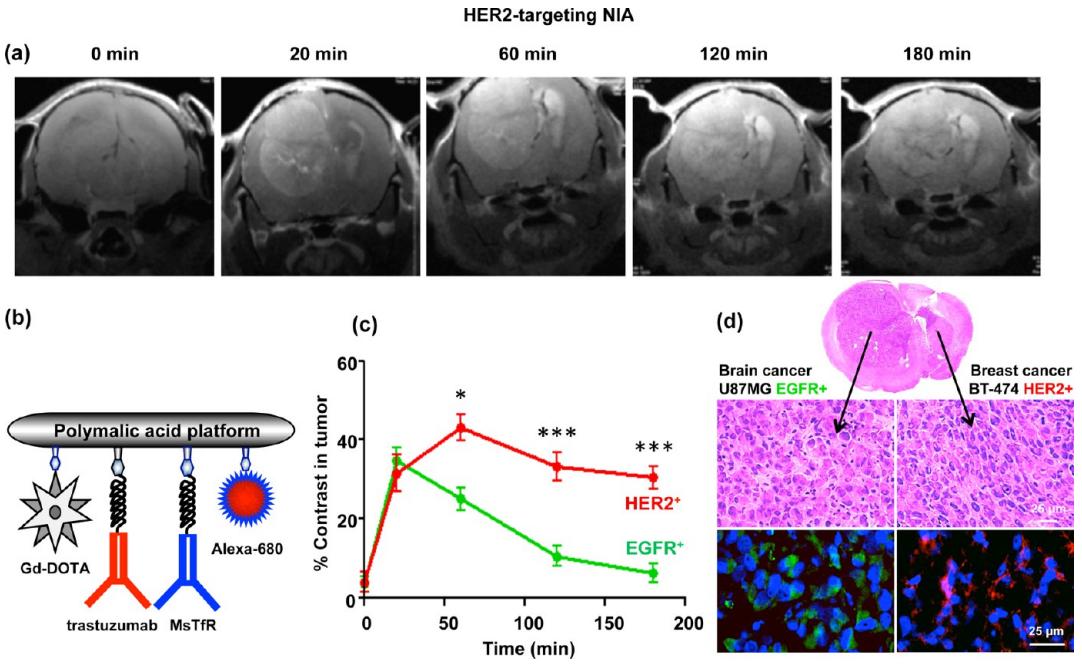

Figure 5. Detection of HER2$^+$ metastatic breast tumor in the presence of EGFR$^+$ GBM (double tumor model) using HER2-targeting NIA. (a) MRI scans of mice with double tumors, a primary GBM (U87MG, EGFR$^+$) in the left hemisphere and metastatic breast cancer (BT-474, HER2$^+$) in the right hemisphere after iv injection of targeted NIA (P/Gd-DOTA/trastuzumab/MsTfR-mAb/Alexa-680). Both tumors showed contrast at 20 min. At later times, only HER2$^+$ tumor retained high contrast due to specific accumulation of targeted agent, whereas little contrast was seen in the EGFR$^+$ nontargeted tumor. (b) Schematic presentation of dual modality (MRI contrast and optical) imaging agents. (c) Quantitative analysis of MRI contrast in the two tumors. High contrast in the targeted HER2$^+$ tumor was maintained beyond 3 h, whereas contrast in the GBM approached the baseline after 3 h (*p < 0.05 at 60 min; ***p < 0.001 at 120 and 180 min). (d) Confirmation of the MRI diagnosis by immunohistochemical analysis. Brain sections showed the presence of two tumors by H&E staining. Brain areas identified by MRI as HER2$^+$ tumor were positive for HER2 (red), and areas not identified as HER2$^+$ were positive for EGFR (green). These results are complementary to the data obtained with EGFR-targeting NIA.

vs PBS-treated control (median survival 29 days for PBS *vs* 48 days for the nanodrug, p < 0.0008). In the third metastatic MDA-MB-468 BM model with EGFR-overexpressing TNBC, nanodrug P/Hu/MsTfR-mAb/EGFR-AON showed the highest, 114%, improvement in survival (median survival 29 days for PBS *vs* 62 days for the nanodrug, p < 0.0006). The AONs against EGFR were designed to inhibit both wild EGFR and mutated EGFRvIII protein that is often overexpressed in primary brain, lung cancer, and TNBC.[29]

After the treatment, tumor samples were dissected from the brain under a microscope using serial hematoxylin and eosin (H&E) stained sections as a guide. By Western blot analysis, expression of HER2 significantly decreased in tumors extracted from HER2-targeting nanodrug-treated mice as compared to PBS-treated controls (Figure 8d and g). Immunostaining agreed well with Western blotting data. In the lung tumor BM model, we observed a decrease in the EGFR expression after treatment with P/Hu/MsTfR-mAb/EGFR-AON using immunostaining and Western analysis for EGFR (Figure 8e and h). Similarly, in a BM model with EGFR$^+$ TNBC, a significant decrease in EGFR expression was seen upon animal treatment with the same nanodrug P/Hu/MsTfR-mAb/EGFR-AON (Figure 8f and i). In all three treated tumor models, there was a significant decrease of activated/phosphorylated Akt (pAkt), which is a pro-survival signaling mediator downstream from both HER2 and EGFR (Figure 8d, e, and f). These data suggest that increased animal survival upon nanodrug treatment was due to the inhibition of targeted genes/proteins and associated suppression of the phosphatidylinositol 3-kinase (PI3K)−Akt pathway.

Interestingly, treatment of all three types of BMs with nanodrugs led to a marked decrease in immunostaining for proteins associated with cancer stem cells, *e.g.*, CD133 and c-Myc (Figure S5). The latter has been also implicated in increased proliferation in various tumors.[30−34] It has been shown that mutated EGFRvIII is highly coexpressed with CD133 and that bispecific antibody EGFRvIIIfl/CD133fl defines the population of cancer stem cells with the highest degree of self-renewal and tumor-initiating ability. As our drug can inhibit both wild type and mutated EGFR, the presented data agree well with recent publication where a bispecific antibody against EFGRvIII and CD133 was able to suppress glioma growth.[29]

Development of new imaging and treatment modalities for brain tumors and BMs requires innovative approaches and new preclinical models. Novel BBB-crossing nanodrugs for systemic treatment of primary GBMs by inhibiting glioma-overexpressed molecular

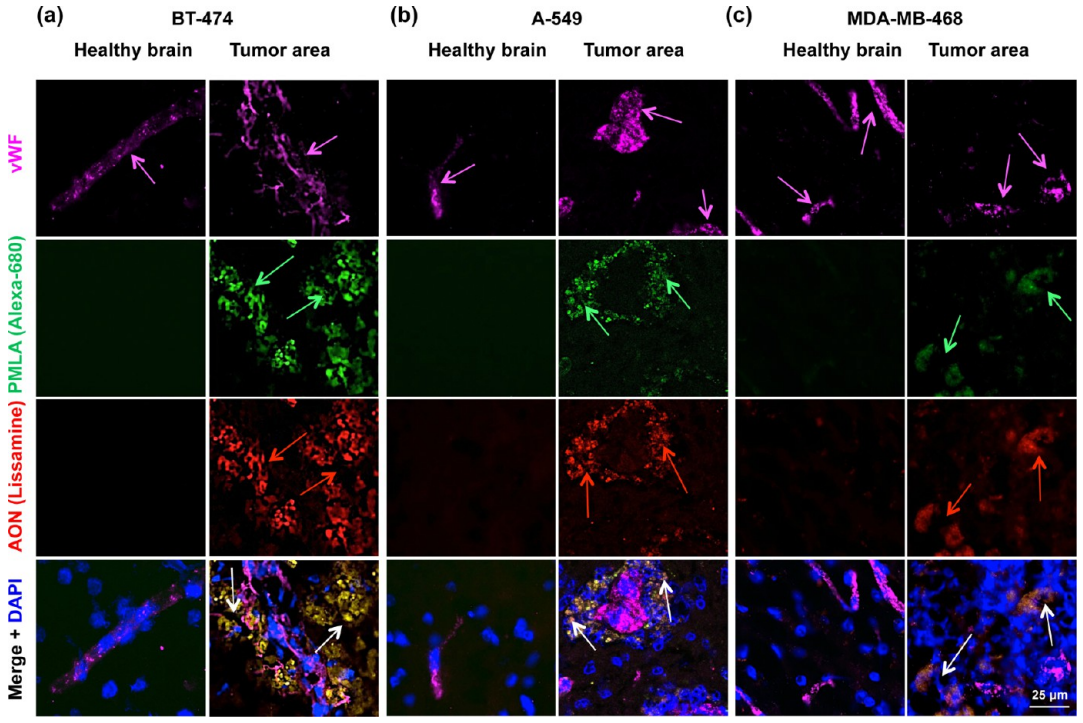

Figure 6. Cytoplasmic delivery of AONs to metastatic brain tumors *in vivo*. (a) Fluorescent microscopy of brain cryostat sections after iv injection of double-labeled nanoconjugate P/mPEG(5%)/LoEt(40%)/EGFR AON-Lissamine(2%)/trastuzumab-(0.2%)/MsTfR(0.2%)/Alexa-680(1%) in mice bearing intracranial breast BT-474 HER2$^+$ tumors. (b and c) Fluorescent microscopy of brain cryostat sections after iv injection of double-labeled nanoconjugate P/mPEG(5%)/LoEt(40%)/EGFR AON-Lissamine(2%)/HuTfR(0.2%)/MsTfR(0.2%)/Alexa-680(1%) in mice bearing EGFR-overexpressing tumors A-549 (lung) and MDA-MB-468 (TNBC). The PMLA platform was labeled green with Alexa-680 (green arrows) and the AONs, red with Lissamine (red arrows). Vessels were labeled magenta by immunostaining for von Willebrand factor (vWF, magenta arrows). Eight hours after iv tail vein injection of nanodrug, mice were euthanized and organs were harvested after intra-arterial PBS perfusion. Brain was excised and immunostained for vWF, and microscopic analysis of sliced brain sections was performed. The nanodrugs were able to extravagate, and both PMLA and AON showed distinct accumulation in the tumor cells in all three xenografts. They display significant colocalization in the tumor cell cytoplasm (yellow; white arrows).

markers are emerging.[35] Magnetic nanomaterials for use by MRI have also been introduced for tumor imaging.[36] However, we wanted to add personalized diagnostic and treatment potential and to develop new biocompatible and biodegradable MRI NIAs that are missing in the clinic, which was emphasized in a recent review.[36] To address this clinical need, we designed nanoscale contrast agents to perform personalized MRI-based diagnosis, which is safe and achievable within a few hours. We have developed new nanoconjugates directly targeting tumor-specific cancer cell biomarkers for noninvasive MRI verification of the brain primary and metastatic tumors. Subsequently, similar targeted nanodrugs against cancer markers were used for specific elimination of tumor cells in several models of BM. The first task was to create reliable and optimized xenogeneic models of HER2$^+$ breast cancer and EGFR$^+$ TNBC and lung cancer, with 100% BM formation in 2−3 weeks after tumor cell inoculation. The only model to achieve this would be by intracranial injections used here. The existing intra-arterial/intravenous BM models are adequate for studying mechanisms of metastasis,[38−40] but may not be suitable for treatment development, as they yield small/micrometastases and low incidence (3−15%) of BM formation.[41] Further, there was no animal model that would use two distinctly different tumors in one brain with independently tunable growth kinetics. However, such a model could constitute a highly accurate test system for the specificity of targeted MRI NIAs that would allow noninvasive biopsy-free differential BM diagnosis. We have optimized stereotactic single and a novel double brain tumor implantation to mimic BM, where different xenograft brain tumors formed with 100% efficiency. Tumor formation was highly selective, and in the double tumor model, no cell migration was seen from one hemisphere to the other after inoculation of a specific type of cells in either brain hemisphere.

Our new model of double human brain tumors in mice mimicking brain metastasis allowed us to develop noninvasive differential tumor diagnostics based on MRI (Figures 4 and 5) and a subsequent efficient BM treatment with nanodrugs. By virtue of mAbs attached to a NIA and ensuring transcytosis through the BBB (anti-TfR) and targeting tumor cell markers for specific cancer cell uptake (anti-HER2 or anti-EGFR), the NIAs with a Gd-DOTA tracer accumulated in BMs and

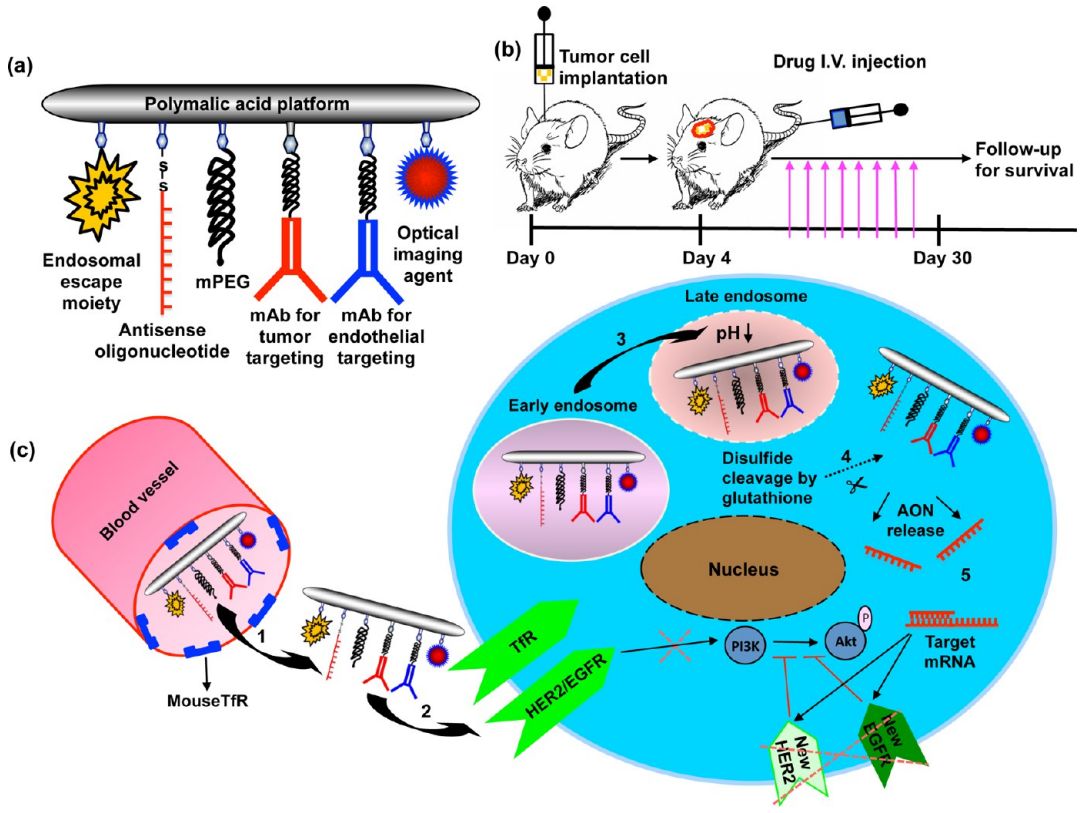

Figure 7. Schematic presentation of nanodrugs and mechanism of action. (a) Functional moieties mPEG, mediating stealth and protection against degradation, LOEt for endosomal escape, and MEA for attachment of antibodies. mAbs and Alexa Fluor 680 are attached to MEA by thioether bonds. AONs are bound to MEA through disulfide linkages. Anti-mouse TfR mAb was used for endothelial targeting and transcytosis; trastuzumab and antihuman TfR mAb were used for active tumor cell targeting. (b) Stereotactic implantation of brain tumors. Nanodrug was injected iv 3 days post tumor inoculation. Nanodrug was injected twice a week, multiple treatments were performed, and animals were followed for survival. (c) Mechanism of action of targeted nanodrugs: (1) Extravasation by endothelial transcytosis after binding to TfR overexpressed on tumor neovascular endothelium. (2) Targeting of cancer cells by specific binding of mAbs to surface receptors and uptake into tumor cells by receptor-mediated endocytosis. (3) Efficient endosomal escape mediated by PMLA-attached LOEt. (4) Release of active AONs after reductive disulfide cleavage by glutathione, abundant in the cytoplasm. (5) Binding of AONs to specific mRNA targets (HER2 and EGFR) inhibits new receptor synthesis and activation of downstream pro-survival PI3K/Akt pathway.

distinguished between different tumor types on MRI. It should be noted that we used the "classical" approach for BBB drug delivery with the anti-TfR antibody, which is already in clinical trials. It was introduced by Pardridge's group, who also developed fusion constructs of therapeutic proteins with specific "Trojan horse" mAbs targeting endogenous BBB receptors such as insulin receptor or TfR.[19] In general, our technology based on a biodegradable and nontoxic PMLA nanoplatform[22,42] can be applied to any molecules crossing the BBB in order to deliver specific agents able to recognize various brain pathological conditions by "MRI virtual biopsy". The Trojan horse constructs and bispecific fusion antibodies containing mAbs to insulin receptor or TfR to cross the BBB can be used for tumor treatment but have significant disadvantages when compared to our nanoconjugates. For imaging, a DOTA formulation of Gd is needed to reduce toxicity, but it cannot be easily attached to antibodies in large quantities, in contrast to PMLA-based polymer. For treatment, molecular Trojan horses and bispecific antibodies can be delivered to tumor cells but would be largely slated for lysosomal degradation because, in contrast to our nanodrugs, they lack endosomal escape capabilities.[37,43]

The specific BM imaging method described here offers "virtual biopsy" without traditional histological diagnosis on biopsies, which are invasive or sometimes impossible for brain tumors.[44] The method of targeted dynamic MRI contrast enhancement was applicable to single and double brain tumors differentially highlighted based on specific cell surface markers, *e.g.*, HER2 or EGFR. Contrast agent was rapidly "washed out" from nontargeted normal brain or irrelevant tumor tissues, leaving highly significant contrast only in the targeted tumors. A single MRI scan appears to be sufficient for diagnosis, optimally around 2−3 h after iv injection of NIA. Therefore, a patient could leave an MRI facility with a noninvasively typed BM within 3 h. If one NIA cannot give a clear diagnosis, an NIA with another targeting specificity could be administered in 12−24 h. Importantly, these NIAs can be easily

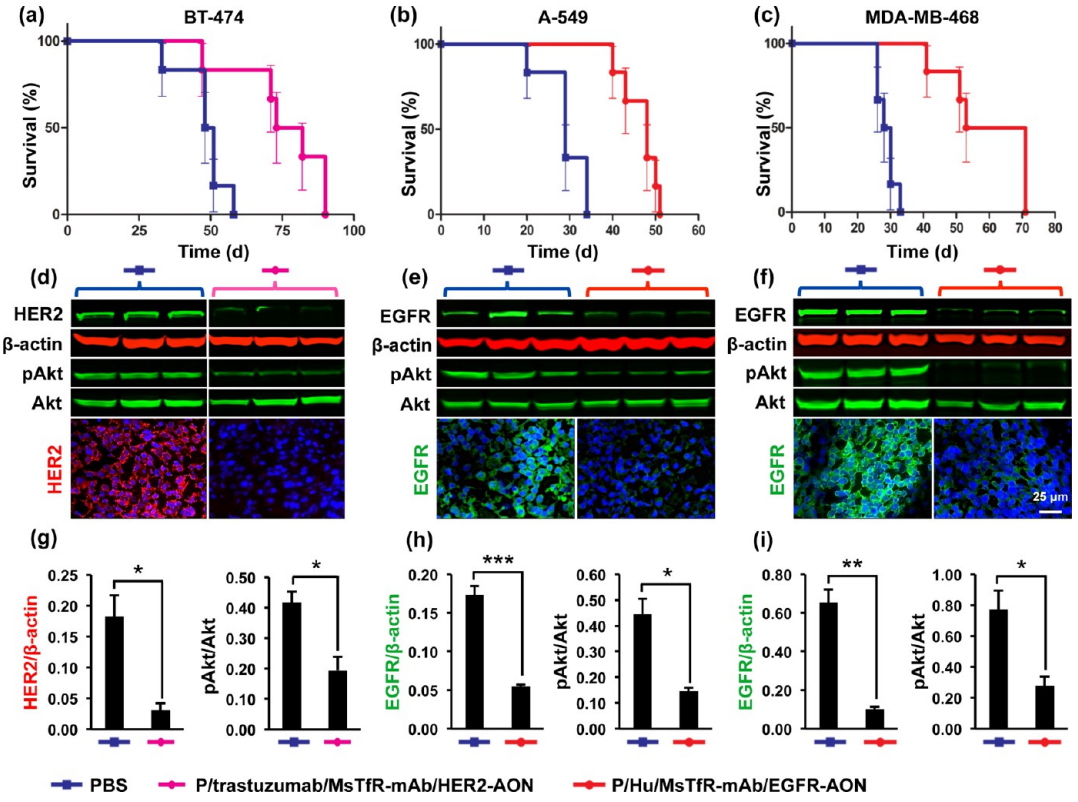

Figure 8. Treatment of breast (HER2$^+$ and TNBC) and lung cancer BMs. (a) Kaplan−Meier animal survival curve for the treatment of HER2$^+$ BT-474 BM. The nanodrug P/trastuzumab/MsTfR-mAb/HER2-AON improved survival by 57% (median survival 77.5 days for nanodrug *vs* 49.5 days for PBS control; $p < 0.005$). (b) P/Hu/MsTfR-mAb/EGFR-AON improved survival of animals with EGFR$^+$ lung cancer BMs by 66% (median survival 48 days for nanodrug *vs* 29 days for PBS control; $p < 0.0008$). (c) P/Hu/MsTfR-mAb/EGFR-AON improved survival of animals with EGFR$^+$ TNBC BM by 114% (median survival 62 days for nanodrug *vs* 29 days for PBS control; $p < 0.0006$). (d−f) Western analysis of tumors excised from mouse brains. β-Actin and total Akt served as loading controls for HER2/EGFR and pAkt, respectively. $N = 3$ tumors in each group. Immunostaining also showed dramatic reduction of respective drug targets in nanodrug-treated *vs* PBS-treated tumors. (g−i) Quantitation of Western blots showed significant reduction of HER2 and pAkt in BT-474 BM upon nanodrug *vs* PBS treatment (g; *$p < 0.05$) and of EGFR and pAkt in lung A-549 BM (h; ***$p < 0.001$ for EGFR and *$p < 0.05$ for pAkt) and in TNBC BM (i; **$p < 0.01$ for EGFR and *$p < 0.05$ for pAkt).

modified with other antibodies to target tumors with different markers.

CONCLUSIONS

A significant advantage of our nanosystem is a possibility to use it not only for imaging but also for the delivery of specific mRNA suppressors (AONs) or other drugs with simple structural manipulations of the nanoplatform for efficient tumor treatment.[35,36] This versatility was illustrated here by successfully treating BMs from breast and lung tumors using different tumor-targeting mAbs (*e.g.*, trastuzumab for HER2$^+$ tumors and anti-human TfR for EGFR$^+$ tumors, Figure 8). For BM treatment, Gd-DOTA in NIAs was just substituted by HER2- or EGFR-specific AONs to block the synthesis of these tumor markers along with an endosomal escape unit for cytoplasmic delivery and PEG for protection. These AONs were delivered to the tumor cell cytoplasm while sparing healthy brain tissue (Figure 6 and S4). They efficiently blocked the synthesis of new HER2 or EGFR and suppressed the activation of the downstream PI3K/Akt signaling pathway. This pro-survival pathway may contribute to apoptosis prevention, regulation of cell cycle progression, and enhanced tumor cell survival.[32,33,45,46] In nanodrug-treated tumors, we found suppression of this important signaling through the inhibition of HER2 or EGFR, exemplified by a significant decrease in pAkt. Inhibition of these important tumor proteins was also associated with reduced expression of some key proliferation and stem cell markers in treated tumors. Whereas some markers displayed changes in some tumors only, reduced immunostaining for c-Myc and CD133 upon nanodrug treatment was a common feature in all three BM models (Figure S5). c-Myc is a key player in HER2- and EGFR-mediated signaling,[47,48] an indicator of tumor proliferation and a cancer stem marker necessary for tumor maintenance and recurrence.[49,50] CD133 is also a tumor stem cell marker associated with circulating cancer cells, tumor chemoresistance, and patient survival.[33,34] Our data suggest that the used nanodrugs inhibited not only tumor markers related to tumorigenicity but also their downstream signaling, important for survival of tumor cells

including cancer stem cells, which play a significant role in chemoresistance and recurrence development. This is especially important for hard to reach and treat BMs. Our nanodrugs thus can deliver specific antibodies, MRI contrast agents, and AONs to specific tumors precisely, which can help in differential diagnosis and treatment of various metastatic brain tumors.

MATERIALS AND METHODS

Reagents. Highly purified poly(β-L-malic acid) was prepared from the culture broth of *Physarum polycephalum* as described.[51] Morpholino-3′-NH2 antisense oligonucleotides 5′-TCGCTCCGGCTCTCCCGATCAATAC-3′ to EGFR and 5′-AGGGAGCCGCAGCTTCATGTCTGTG-3′ to HER2 were custom-made by Gene Tools. Mouse anti-human transferrin receptor (TfR, CD71) mAb clone RVS10, IgG1, was from Southern Biotech, and rat anti-mouse TfR mAb clone R17217, IgG2aκ, was from BioLegend. The primary antibodies against the following markers were used for immunohistochemistry: c-Myc, EGFR, HER2, von Willebrand factor (all from Abcam), and CD133 (Millipore). For Western blot analysis antibodies were used against EGFR, phosphorylated and total Akt, and β-actin and glyceraldehyde 3-phosphate dehydrogenase (GAPDH) as gel loading controls (Cell Signaling Technology). Secondary antibodies included anti-mouse IgG FITC (Millipore), anti-rabbit IgG Alexa-488 (Thermo Scientific), anti-rat IgG Texas Red (BD Biosciences), anti-rat IgG FITC (Jackson Immuno Research Lab), and anti-rabbit, and anti-sheep IgG Alexa Fluor 680 (Thermo Scientific). Cetuximab (Erbitux) and trastuzumab (Herceptin) were from Bristol-Myers Squibb and Genentech, Inc., respectively. mPEG5000-amine (mPEG) and maleimide-PEG3400-maleimide MAL-PEG3400-MAL were obtained from Laysan Bio. NH_2-Leu-OEt (LOEt) and *N*-succinimidyl-3-(2-pyridyldithio)propionate (SPDP) were from Bachem Americas, Inc. Alexa Fluor 680 C2 maleimide (Alexa-680) was purchased from Life Technologies. Human and mouse TfR antigens were obtained from Protein Expression Center, California Institute of Technology. Azido-monoamide-DOTA was purchased from Macrocyclics, Inc. 3-(2-Pyridyldithio)-propionate (PDP) was synthesized as described.[54] Unless otherwise indicated, all chemicals and solvents of highest purity were purchased from Sigma-Aldrich.

Analytical Methods for Synthesis of NIA. The conjugation reaction of Gd-DOTA amine and 2-MEA with PMLA was followed by thin layer chromatography (TLC) on precoated silica gel 60 F254 aluminum sheets and visualization of spots by UV light and/or by ninhydrin staining. Size exclusion chromatography was performed on an Elite LaChrom analytical system with an L 2455 diode array detector (Hitachi), and MW was measured using either BioSep-SEC-S 4000 and/or PolySep-GFC-P 4000 (300 × 7.80 mm) (Phenomenex) with 50 mM sodium phosphate buffer pH 6.8 as a mobile phase and polystyrenesulfonates as molecular weight standards. Thiol residues attached to PMLA were assayed by the method of Ellman. Enzyme-linked immunosorbent assay (ELISA) was used to determine the functional activity of conjugated antibody using an ELISA protein detector kit (KPL, Inc.). The amount of Gd in nanoconjugates was determined by ICP-MS at UCLA. The presence of free Gd was detected with Xylenol orange, a complexometric indicator as reported.[52] For quantification of mPEG, the amount of complexation with ammonium ferrothiocyanate and extraction with chloroform was obtained by absorbance reading at 510 nm.[53] The content of monoclonal IgG antibody (mAb) was determined by a Pierce BCA protein assay kit (Thermo Scientific). Unlabeled antibodies were used to generate a standard curve. Quantification of malic acid in nanoconjugates was performed by the malate dehydrogenase assay.[51] Percentage (%) of the nanoconjugate loading with morpholino AON, mAb, or mPEG5000 was calculated by using the formula % = 100(μmol ligand)/(μmol malic acid).

Synthesis of Gd-DOTA with Amine Side Chain. Preparation of metal complex: One equivalent of azido-monoamide-DOTA (0.56 mmol) was dissolved in water (4 mL), and a slight stoichiometric excess of gadolinium(III) acetate (0.61 mmol) in water (4 mL) was added dropwise. The solution was stirred at room temperature (RT) while maintaining the pH between 6 and 7 by addition of 1 M NaOH. The reaction mixture was then stirred for 48 h. The free Gd ions were removed with Chelex 100 resin. Reaction yield was 90%. Reduction of azide to amine: Azido Gd-DOTA (0.5 mmol) was dissolved in water (25 mg/mL), and 10% (w/w) of 10% Pd−C (palladium on carbon) was added. Hydrogen gas was filled into a balloon and exposed to the reaction mixture. The reaction was complete after 5 h, as confirmed by TLC (n-butanol/water/acetic acid, 1:1:1) and ninhydrin staining. The reaction mixture was filtered through a calcite pad, washed with water, and freeze-dried to obtain a white solid. The reaction yield was 96%.

Synthesis of Preconjugate-1. *N*-Hydroxysuccinimide (NHS; 0.62 mmol) and *N*,*N*′-dicyclohexylcarbodiimide (DCC; 1 mmol) dissolved in 2 mL of dimethylformamide (DMF) were added consecutively to the solution of 72 mg of PMLA (0.62 mmol with regard to malyl units) dissolved in 1.5 mL of anhydrous acetone under vigorous stirring at RT. After stirring at RT for 3 h to complete the activation of carboxyl groups, the reaction mixture was filtered and acetone was removed using a rotary evaporator. MEA (0.05 mmol in DMF; 100 μL, 5 mol % with regard to malyl units) was added to the reaction mixture followed by an equivalent amount of triethylamine (TEA), and reaction mixture was stirred at RT for 45 min. A solution of Gd-DOTA, 20 mol % with regard to malyl units, was dissolved in 100 mM sodium phosphate and 150 mM NaCl, pH 6.8 phosphate buffer and was added to the reaction mixture at RT under stirring followed by addition of 0.20 mmol of TEA. The reaction was further stirred for 2 h. After centrifugation at 1500*g* for 10 min the clear supernatant was passed over a Sephadex PD-10 column (GE Healthcare) pre-equilibrated with deionized (DI) water. The product-containing fractions were collected and freeze-dried. The amount of Gd-DOTA was found to be 10−12% with regard to malyl units after ICP-MS determination, and the amount of thiol was found to be 3−4%, estimated by Ellman's reagent. The reaction yield was 63%.

Synthesis of Preconjugate-2. After acid activation of PMLA (116 mg, 1 mmol) by NHS and DCC as described for Preconjugate-1, 0.05 mmol of mPEG5000-NH_2 (in 1.0 mL of DMF, 5 mol % with regard to malyl units) was added followed by 0.05 mmol of TEA, and the reaction mixture was stirred at RT until the reaction was complete according to TLC and a negative ninhydrin test (reaction finishes usually in 45 min). A solution of L-leucine ethyl ester (LOEt) hydrochloride (200 mM in DMF, 40 mol % with regard to malyl units) was added dropwise at RT under stirring followed by the addition of 0.4 mmol of TEA. The reaction was complete after 2 h according to TLC (R_f = 0 for the polymer conjugate, R_f = 0.67 for LOEt; *n*-butanol/acetic acid/water, 4:2:2), and visualization of spots was by ninhydrin. Finally, 2-MEA (0.10 mmol in DMF; 100 μL, 10 mol % with regard to malyl units) was added to the reaction mixture. After stirring at RT for 45 min, a solution (100 mM sodium phosphate and 150 mM NaCl, pH 6.8) was added and the reaction mixture was stirred at RT for 30 min. After centrifugation at 1500*g* for 10 min the clear supernatant was passed over PD-10 Sephadex columns (GE Healthcare) pre-equilibrated with DI water. The product-containing fractions were collected and freeze-dried. The reaction yield was 67%.

Synthesis of NIA for MRI. A solution of a mixture of anti-mouse (MsTfR) and cetuximab or trastuzumab mAb/PEG3400/maleimide (6 mg each) at a concentration 4 mg/mL in 100 mM sodium phosphate buffer containing 150 mM NaCl (pH 6.3) synthesized as described above was added to 8 mg of Preconjugate-1 at a concentration of 4 mg/mL in the same buffer. The reaction mixture was stirred for 2 h at RT and was monitored by SEC-HPLC. Alexa-680 at 1 mg/mL was added, and

the reaction mixture was stirred for 1 h at RT. The stock solution of Alexa-680 was prepared in DMF to preserve the maleimide functional group, as maleimde groups are relatively less stable in aqueous solutions when stored for long periods of time. DMF is low in the final reaction mixture (~5−10%). Published data confirm that up to 40% DMF does not alter the antibody activity, which is corroborated by our routine analysis of the functional activity of conjugated antibodies by ELISA and/or flow cytometry analysis. To allow for blocking of the remaining −SH groups, excess PDP was added and allowed to react for 30 min at RT. The product was concentrated by centrifugation through a Vivaspin 20 membrane filter, 30 kDa cutoff at 1500*g* (Sartorius Stedim Biotech), to the final volume of 1−2 mL before purification over Sephadex G-75 pre-equilibrated with PBS, pH 7.4. Product-containing fractions were isolated, combined, and concentrated *via* membrane filtration. Reaction yield was 80−90%. A similar procedure was used for the synthesis of P/cetuximab(0.12%)/MsTfR-mAb(0.12%)/rhodamine(1%)/Gd-DOTA(10−12%).

Synthesis of Nanodrug for Treatment. After conjugating antibodies to Preconjugate-2 by the method described above for conjugation with Preconjugate-1, 10 mg of AON-PDP dissolved in sodium phosphate buffer (100 mM, 150 mM NaCl, pH ~5.5) was added, and the mixture was allowed to stir for 16 h at 4 °C. The reaction was followed by SEC-HPLC, and the amount of AON bound to mAb-Preconjugate-2 was monitored. To allow for blocking of remaining −SH groups, excess PDP (30 μL, from a stock solution of 110 mg/mL in DMF) was added and allowed to react for 30 min at RT. The product was concentrated by centrifugation through a Vivaspin 20 membrane filter, 30 kDa cutoff at 1500*g* (Sartorius Stedim Biotech), to a final volume of 2 mL before purification over Sephadex G-75 pre-equilibrated with PBS, pH 7.4. Product-containing fractions were isolated, combined, and concentrated *via* membrane filtration.

Fluorescent Dye Labeling of Nanodrugs. Fluorescent dye dissolved in DMF at 1 mg/mL was added to the solution of desired conjugates (2−4 mg/mL) in 100 mM sodium phosphate buffer with 150 mM NaCl, pH 5.5. The reaction mixture was stirred at RT for 1 h and passed over Sephadex G-75 pre-equilibrated with PBS. The product was concentrated *via* membrane filtration. For all NIAs, fluorescent dye labeling was performed before blocking of excess free thiol groups by PDP.

Synthesis of Nanoconjugates for the Treatment of the Brain Metastases of Lung, TNBC, and HER2 Positive Breast Cancer. *Synthesis of PDP-AONs (for all AONs).* Morpholino antisense oligonucleotides (AON; 3′ amine modified) (25 mg, 0.0028 mmol) were dissolved in 1.5 mL of DMF and 500 μL of PBS. A solution of SPDP (9.37 mg, 0.03 mmol) in a 1:1 mixture of DMF/MeOH (400 μL) was added to the AON solution. The reaction mixture was stirred at RT for 1 h. The reaction was followed by TLC and the ninhydrin test as well as reverse phase HPLC. The solvent was reduced to 0.5−1 mL by rotary evaporation, MeOH was added to make a final volume of 2 mL, and purified over Sephadex-LH20. Fractions were collected and the solvent was evaporated to dryness. The product was dissolved in water and freeze-dried. The reaction yield was 80−95%.

Synthesis of Antibody-PEG3400-Maleimide (for All Antibodies). To the solution of mAb (5 mg, ~33 nmol, M_r ~150 kDa) dissolved in 2 mL of 100 mM sodium phosphate buffer containing 150 mM NaCl pH 5.5 was added tris(2-carboxyethyl)phosphine hydrochloride (TCEP, to a final concentration of 5 mM, prepared as a 50 mM solution in water). The mixture was incubated for 30 min at RT. TCEP was removed using Sephadex PD10, and the reduced antibody was immediately added dropwise to MAL-PEG3400-MAL (10 mmol) dissolved in 1 mL of freshly prepared, sterile 100 mM sodium phosphate buffer with 150 mM NaCl (pH 5.5). The reaction mixture was stirred at RT for 1 h and then was concentrated using a centrifuge membrane filter (Vivascience, cutoff 30 kDa, 20 mL, 100 mM sodium phosphate buffer containing 150 mM NaCl, ~pH 5.5) and purified over Sephadex G75 pre-equilibrated with 100 mM sodium phosphate buffer and 150 mM NaCl, pH 6.3. Pure fractions containing antibody were collected, adjusted to 4 mg/mL, and used in the next step. The reaction yield was 70−85%.

Quantification of AONs in the Nanoconjugate. To quantify morpholino AON, the disulfide spacer of the nanopolymer platform was cleaved to release AON by the addition of 100 mM dithiothreitol at pH 7.4, 1 h at RT. Reverse phase HPLC at 260 nm with free morpholino AON as standards was carried out for quantification using C_{18}, 5 μm, size 4.6 mm × 250 mm, with a gradient of water (0.1% TFA) to acetonitrile (0.1% TFA) at a flow rate of 1 mL/min.

Hydrodynamic Diameter and Zeta Potential Measurement. Synthesized conjugates were characterized with respect to their size and ζ potential using a Zetasizer Nano ZS90 (Malvern Instruments). For the particle size measurements at 25 °C, the solutions were prepared in PBS at a concentration of 2 mg/mL. For the measurement of the ζ potential, the concentration of the sample dissolved in a 10 mM NaCl solution was 2 mg/mL, and the voltage applied was 150 mV. Data represent the mean of three measurements ± standard deviation.

MRI Measurements. To study the accumulation of an MRI contrast agent in the tumor tissue, mice were anesthetized by inhalation of isoflurane (2−4% to effect) inside an induction chamber. Contrast agents dissolved in PBS at a dose of 0.1 mmol Gd/kg were administered *via* the tail vein using a 1 mL syringe and a 30-gauge needle. Anesthesia was maintained during measurements by nose cone administration of 1.5−1.8% isoflurane. The mouse bed was heated to prevent cooling of the mice during anesthesia. Breathing was regulated in the range of 35−40 breaths/min during the measurements by slightly increasing or decreasing the percentage of isoflurane. Images were recorded at time points of 0, 20, 60, 120, and 180 min after contrast agent injection. The MRI acquisition was performed when tumors were 2−4 mm in diameter. Spin−echo images of the entire brain were acquired. Axial slices were positioned over the tumor region. A multislice multiecho sequence (8 spin−echos) was used with a TR = 450 ms. Slices were acquired with a 1.0 mm thickness for a 1.8 × 1.8 cm field of view with a 256 × 196 matrix size providing an in-plane resolution of 70 × 92 μm/pixel. T1 values of the samples were measured from ROI using a single-exponential fitting of the intensity for different repetition time scans. In this case, the in-plane resolution was 234 × 92 μm/pixel. Animals underwent MRI scanning on a Bruker BioSpec 94/20USR 9.4 T small-animal scanner (Bruker Biospin MRI GmbH). Each animal was placed inside a transmission whole body coil (T10325 V3, Bruker Biospin MRI GmbH) with a four-channel surface array coil (T11071 V3, Bruker Biospin MRI GmbH) positioned over the brain. The transmission body coil was used for all radio frequency transmission; the surface coil was used for detection.

MR Image Quantification. To quantify image enhancement over time, we developed an unbiased image analysis program. T1-weighted images (three contiguous slices through the center of each tumor) collected before and 20, 60, 120, and 180 min immediately after iv injection were analyzed. For each time point, MRI scans of the whole brain included several slices of 1.0 mm thickness. We chose a minimum of three slices for each time point. We traced the regions of interest for the brain tumor and chose reference regions for normal brain on the same plane (Figure S3). On each slice, multiple ROI were selected. At least three ROI were used for each analysis. MRI images were stored in TIFF format and analyzed by Leica MM AF 1.6 software. An average intensity/pixel was calculated for each ROI individually. The presented data refer to intensity ratios with reference to normal brain tissue and are given as mean values ± standard error of mean (SEM). They are shown as a function of the time elapsed after the injection of the contrast agents.

Cell Lines and Culture Conditions. Human breast cancer cell lines MDA-MB-468 (TNBC, EGFR+), BT-474 (HER2+), and human lung cancer cell line A-549 (EGFR+) were obtained from ATCC. Primary glioblastoma U87MG cell line was a gift from Drs. Webster Cavenee and Frank Furnari (UC San Diego) and was cultured in minimum essential medium (MEM) supplemented with 10% fetal bovine serum (FBS), 1% MEM nonessential amino acids, 1 mM sodium pyruvate, and 2 mM L-glutamine. MDA-MB-468 was cultured in Leibovitz's L-15 medium with 10% FBS at 37 °C without CO_2. BT-474 and A549 cells were cultured in L-15 and

F-12K medium, respectively, supplemented with 10% FBS and antibiotics/antimycotics at 37 °C with CO_2.

Tumor Xenografts and Nanodrug Treatment. All experiments with animals were performed in strict accordance with the protocols approved by the Cedars-Sinai Medical Center Institutional Animal Care and Use Committee (IACUC). Athymic NCr-nu/nu female mice were obtained from NCI-Frederick. Double tumors were stereotactically implanted as follows: $EGFR^+$ U87MG GBM cells at 2.5×10^4 into the left basal ganglia, and $HER2^+$ BT-474 cells at 1×10^5 into the right basal ganglia field of mouse brain. Three cell cultures were intracranially inoculated. We developed models of metastatic brain tumors using a lung (A-549) and a hormone-dependent (BT-474) or -independent (TNBC, MDA-MB-468) breast cancer cell lines. The number of animals per group for each tumor type was $n = 5-8$. For hormone-dependent BT-474 tumors, a 0.72 mg, 90-day-release estrogen pellet was aseptically placed under the skin 7 days before BT-474 tumor cell implantation. MDA-MB-468 cells were stereotactically implanted at 1.5×10^6 into the right basal ganglia field of the mice. BT-474 and A-549 cells were stereotactically implanted at 1×10^5 and 5×10^5, respectively.

Mice bearing the metastatic brain tumors, either BT-474, MDA-MB-468, or A-549 cells, were treated with nanodrugs every 3 days intravenously *via* tail vein starting 3 days post tumor inoculation. The mice bearing lung tumor or TNBC in the brain were treated 8 times, and the mice bearing HER2+ tumors were treated 16 times as per the clinical regime of trastuzumab.[26] All animals were followed for survival post-treatment. PBS as a drug solvent was used as a negative control and administered the same way.

Xenogen IVIS 200 Mouse Imaging. For the assessment of drug distribution and localization in nude mice, animals were imaged using a Xenogen IVIS 200 imager under isoflurane anesthesia at different time points (before and after drug administration). Mice were euthanized, and drugs were washed out from circulation by intra-arterial PBS perfusion. Tumor, brain, and other major organs were harvested, and their fluorescence intensities analyzed by Xenogen Living Image software, version 2.50 (WaveMetrix).

Immunohistochemistry. Along with hematoxylin and eosin (H&E) staining, fluorescence immunohistochemistry was used with various antibodies. After the MRI experiments animals were euthanized, and harvested brains were embedded in OCT tissue freezing medium (Tissue Tek) and frozen in liquid nitrogen. Frozen tissue blocks were sectioned at 7–10 μm thickness using a Leica CM 3050S cryostat. Before staining, tissue sections were air-dried at RT, fixed with ice-cold acetone for 10 min, and then rinsed three times with PBS. Sections were incubated in a humidified chamber with blocking buffer (4% normal goat serum, 4% normal donkey serum, 1% BSA, and 0.1% Triton X-100 in PBS) for 1 h at RT to block nonspecific sites. The blocked sections were incubated overnight at 4 °C with primary antibodies diluted in staining buffer and later washed with PBS. Secondary antibodies for double or triple labeling were incubated for 1 h, and sections mounted with Prolonged Gold Antifade (Thermo Scientific) mounting medium containing DAPI. Images were captured using a Leica DM6000B microscope (Germany).

Western Blot Analysis. The brain samples from survival studies were used to determine the fate of targeted receptors and downstream signaling intermediates upon treatment. Whole mouse brain was embedded in OCT, and cryosections were stained with H&E. The H&E slides were used as guides to identify and excise tumor regions from mouse brains. MDA-MB-468, BT-474, and A-549 metastatic brain tumor-bearing mice were treated with nanodrugs (Table 1). Tissue lysates were prepared using T-PER (Thermo Scientific) supplemented with phosphatase and cOmplete EDTA-free, proteinase inhibitor cocktail (Roche) and analyzed by Western blotting to detect EGFR, phosphorylated (pAkt), and total Akt, as well as β-actin and GAPDH as gel loading controls. For two-color quantitative Western analysis, the blots were probed simultaneously with two primary antibodies from different hosts, followed by incubation with infrared dye-conjugated secondary antibodies. The membranes were scanned in an Odyssey CLx (LICOR Biosciences). Quantification of Western blots was performed using Image Studio Lite (version 4.0) software. The blots were probed for products of two housekeeping genes, β-actin and GAPDH. Both proteins showed comparable expression in all samples. β-Actin was chosen for normalizing the blots for HER2 or EGFR expression. Total Akt protein was used to normalize pAkt expression. The graphs represent the ratios of HER2 or EGFR to β-actin or pAkt to Akt expression.

Cell Surface Staining for Flow Cytometry. The cells were trypsinized and washed with PBS supplemented with 2% FBS. They were costained by incubation with P/Gd-DOTA/cetuximab-Rh/MsTfR-mAb containing rhodamine-conjugated cetuximab (2.5 μg/mL) for 30 min at 4 °C. Washed cells fixed with 2% paraformaldehyde were imaged using BD LSRII at Cedars-Sinai Flow Cytometry Core and analyzed using flow software (version 2.5.1). Similar flow cytometry experiments were performed with BT-474 HER2+ cells incubated with P/Gd-DOTA/trastuzumab/MsTfR-mAb/Alexa-680 (2.5 μg/mL). For validation of specificity, competition assays were performed with MDA-MB-468 cells by pretreatment with a 10-fold higher concentration of free unconjugated cetuximab (25 μg/mL) for 30 min. Then, P/Gd-DOTA/cetuximab-Rh/MsTfR-mAb or free cetuximab conjugated to rhodamine was added for another 45 min. All incubations were at 4 °C. PBS-treated cells were included as a negative control.

Statistical Analysis. GraphPad Prism3 (GraphPad Software) was used to plot Kaplan–Meier survival curves (logrank test). Data are presented as mean ± SEM. Student's *t* test was used to calculate statistical significance of the data in two-group comparisons, and ANOVA with Bonferroni post-test for three-group comparisons. The significance level was set at $p < 0.05$.

Conflict of Interest: The authors declare the following competing financial interest(s): Drs. Ljubimova, Black, Ljubimov, and Holler are shareholders of Arrogene Inc.

Acknowledgment. The paper is dedicated to Dr. Holler's anniversary and 50 years of work in science. We thank Drs. W. Cavenee and F. Furnari, University of California San Diego, for U87MG cells, and Dr. R. K. Gangalum, University of California Los Angeles, for TEM measurements. This work was supported by NIH U01 CA151815, NIH R01 CA136841, NIH R01 CA188743, NIH R01 EY013431, Arrogene Inc. grants, and Martz Translational Breast Cancer Research Fund.

Supporting Information Available: Five supplementary figures are available. The Supporting Information is available free of charge on the ACS Publications website at DOI: 10.1021/acsnano.5b01872.

REFERENCES AND NOTES

1. Steeg, P. S.; Camphausen, K. A.; Smith, Q. R. Brain Metastases as Preventive and Therapeutic Targets. *Nat. Rev. Cancer* **2011**, *11*, 352–363.
2. Khanfir, A.; Lahiani, F.; Bouzguenda, R.; Ayedi, I.; Daoud, J.; Frikha, M. Prognostic Factors and Survival in Metastatic Breast Cancer: A Single Institution Experience. *Rep. Pract. Oncol. Radiother.* **2013**, *18*, 127–132.
3. Ranjan, T.; Abrey, L. E. Current Management of Metastatic Brain Disease. *Neurotherapeutics* **2009**, *6*, 598–603.
4. Lu, J.; Steeg, P. S.; Price, J. E.; Krishnamurthy, S.; Mani, S. A.; Reuben, J.; Cristofanilli, M.; Dontu, G.; Bidaut, L.; Valero, V.; *et al*. Breast Cancer Metastasis: Challenges and Opportunities. *Cancer Res.* **2009**, *69*, 4951–4953.
5. Vona-Davis, L.; Rose, D. P.; Gadiyaram, V.; Ducatman, B.; Hobbs, G.; Hazard, H.; Kurian, S.; Abraham, J. Breast Cancer Pathology, Receptor Status, and Patterns of Metastasis in a Rural Appalachian Population. *J. Cancer Epidemiol.* **2014**, *2014*, 170634.
6. Lin, N. U.; Amiri-Kordestani, L.; Palmieri, D.; Liewehr, D. J.; Steeg, P. S. CNS Metastases in Breast Cancer: Old Challenge, New Frontiers. *Clin. Cancer Res.* **2013**, *19*, 6404–6418.
7. Eldredge, H. B.; Denittis, A.; Duhadaway, J. B.; Chernick, M.; Metz, R.; Prendergast, G. C. Concurrent Whole Brain Radiotherapy and Short-Course Chloroquine in Patients with Brain Metastases: A Pilot Trial. *J. Radiat. Oncol.* **2013**, *2*, 315–321.

8. Nayak, L.; Lee, E. Q.; Wen, P. Y. Epidemiology of Brain Metastases. *Curr. Oncol. Rep.* **2012**, *14*, 48–54.
9. Baselga, J. Targeting Tyrosine Kinases in Cancer: The Second Wave. *Science* **2006**, *312*, 1175–1178.
10. Renfrow, J. J.; Lesser, G. J. Molecular Subtyping of Brain Metastases and Implications for Therapy. *Curr. Treat. Options Oncol.* **2013**, *14*, 514–527.
11. Lin, N. U.; Claus, E.; Sohl, J.; Razzak, A. R.; Arnaout, A.; Winer, E. P. Sites of Distant Recurrence and Clinical Outcomes in Patients with Metastatic Triple-Negative Breast Cancer: High Incidence of Central Nervous System Metastases. *Cancer* **2008**, *113*, 2638–2645.
12. Schouten, L. J.; Rutten, J.; Huveneers, H. A.; Twijnstra, A. Incidence of Brain Metastases in a Cohort of Patients with Carcinoma of the Breast, Colon, Kidney, and Lung and Melanoma. *Cancer* **2002**, *94*, 2698–2705.
13. Brabletz, T.; Lyden, D.; Steeg, P. S.; Werb, Z. Roadblocks to Translational Advances on Metastasis Research. *Nat. Med.* **2013**, *19*, 1104–1109.
14. Gallego Perez-Larraya, J.; Hildebrand, J. Brain Metastases. *Handb. Clin. Neurol.* **2014**, *121*, 1143–1157.
15. Jia, W.; Lu, R.; Martin, T. A.; Jiang, W. G. The Role of Claudin-5 in Blood-Brain Barrier (BBB) and Brain Metastases (Review). *Mol. Med. Rep.* **2014**, *9*, 779–785.
16. Lin, N. U. Targeted Therapies in Brain Metastases. *Curr. Treat. Options Neurol.* **2014**, *16*, 276.
17. Inoue, S.; Patil, R.; Portilla-Arias, J.; Ding, H.; Konda, B.; Espinoza, A.; Mongayt, D.; Markman, J. L.; Elramsisy, A.; Phillips, H. W.; *et al*. Nanobiopolymer for Direct Targeting and Inhibition of EGFR Expression in Triple Negative Breast Cancer. *PLoS One* **2012**, *7*, e31070.
18. Markman, J. L.; Rekechenetskiy, A.; Holler, E.; Ljubimova, J. Y. Nanomedicine Therapeutic Approaches to Overcome Cancer Drug Resistance. *Adv. Drug Delivery Rev.* **2013**, *65*, 1866–1879.
19. Pardridge, W. M. Blood-Brain Barrier Drug Delivery of IgG Fusion Proteins with a Transferrin Receptor Monoclonal Antibody. *Expert Opin. Drug Delivery* **2015**, *12*, 207–222.
20. Bickel, U.; Yoshikawa, T.; Pardridge, W. M. Delivery of Peptides and Proteins through the Blood-Brain Barrier. *Adv. Drug Delivery Rev.* **2001**, *46*, 247–279.
21. Daniels, T. R.; Bernabeu, E.; Rodriguez, J. A.; Patel, S.; Kozman, M.; Chiappetta, D. A.; Holler, E.; Ljubimova, J. Y.; Helguera, G.; Penichet, M. L. The Transferrin Receptor and the Targeted Delivery of Therapeutic Agents against Cancer. *Biochim. Biophys. Acta* **2012**, *1820*, 291–317.
22. Ljubimova, J. Y.; Portilla-Arias, J.; Patil, R.; Ding, H.; Inoue, S.; Markman, J. L.; Rekechenetskiy, A.; Konda, B.; Gangalum, P. R.; Chesnokova, A.; *et al*. Toxicity and Efficacy Evaluation of Multiple Targeted Polymalic Acid Conjugates for Triple-Negative Breast Cancer Treatment. *J. Drug Target.* **2013**, *21*, 956–967.
23. Lee, B. S.; Fujita, M.; Khazenzon, N. M.; Wawrowsky, K. A.; Wachsmann-Hogiu, S.; Farkas, D. L.; Black, K. L.; Ljubimova, J. Y.; Holler, E. Polycefin, a New Prototype of a Multifunctional Nanoconjugate Based on Poly(β-L-Malic Acid) for Drug Delivery. *Bioconjugate Chem.* **2006**, *17*, 317–326.
24. Inoue, S.; Ding, H.; Portilla-Arias, J.; Hu, J.; Konda, B.; Fujita, M.; Espinoza, A.; Suhane, S.; Riley, M.; Gates, M.; *et al*. Polymalic Acid-Based Nanobiopolymer Provides Efficient Systemic Breast Cancer Treatment by Inhibiting Both HER2/Neu Receptor Synthesis and Activity. *Cancer Res.* **2011**, *71*, 1454–1464.
25. Allard, M.; Doucet, D.; Kien, P.; Bonnemain, B.; Caille, J. M. Experimental Study of DOTA-Gadolinium. Pharmacokinetics and Pharmacologic Properties. *Invest. Radiol.* **1988**, *23*, S271–274.
26. Pestalozzi, B. C.; Brignoli, S. Trastuzumab in CSF. *J. Clin. Oncol.* **2000**, *18*, 2349–2351.
27. Sun, M.; Behrens, C.; Feng, L.; Ozburn, N.; Tang, X.; Yin, G.; Komaki, R.; Varella-Garcia, M.; Hong, W. K.; Aldape, K. D.; *et al*. HER Family Receptor Abnormalities in Lung Cancer Brain Metastases and Corresponding Primary Tumors. *Clin. Cancer Res.* **2009**, *15*, 4829–4837.
28. Hu, J.; Ljubimova, J. Y.; Inoue, S.; Konda, B.; Patil, R.; Ding, H. Espinoza, A.; Wawrowsky, K. A.; Patil, C.; Ljubimov, A. V.; *et al*. Phosphodiesterase Type 5 Inhibitors Increase Herceptin Transport and Treatment Efficacy in Mouse Metastatic Brain Tumor Models. *PLoS One* **2010**, *5*, e10108.
29. Emlet, D. R.; Gupta, P.; Holgado-Madruga, M.; Del Vecchio, C. A.; Mitra, S. S.; Han, S. Y.; Li, G.; Jensen, K. C.; Vogel, H.; Xu, L. W.; *et al*. Targeting a Glioblastoma Cancer Stem-Cell Population Defined by EGF Receptor Variant III. *Cancer Res.* **2014**, *74*, 1238–1249.
30. Frese, K. K.; Tuveson, D. A. Maximizing Mouse Cancer Models. *Nat. Rev. Cancer* **2007**, *7*, 645–658.
31. Brugnoli, F.; Grassilli, S.; Piazzi, M.; Palomba, M.; Nika, E.; Bavelloni, A.; Capitani, S.; Bertagnolo, V. In Triple Negative Breast Tumor Cells, PLC-β2 Promotes the Conversion of CD133high to CD133low Phenotype and Reduces the CD133-Related Invasiveness. *Mol. Cancer* **2013**, *12*, 165.
32. Moelling, K.; Schad, K.; Bosse, M.; Zimmermann, S.; Schweneker, M. Regulation of Raf-Akt Cross-Talk. *J. Biol. Chem.* **2002**, *277*, 31099–31106.
33. Chautard, E.; Ouedraogo, Z. G.; Biau, J.; Verrelle, P. Role of Akt in Human Malignant Glioma: From Oncogenesis to Tumor Aggressiveness. *J. Neurooncol.* **2014**, *117*, 205–215.
34. Nadal, R.; Ortega, F. G.; Salido, M.; Lorente, J. A.; Rodríguez-Rivera, M.; Delgado-Rodríguez, M.; Macià, M.; Fernández, A.; Corominas, J. M.; Garcia-Puche, J. L.; *et al*. CD133 Expression in Circulating Tumor Cells from Breast Cancer Patients: Potential Role in Resistance to Chemotherapy. *Int. J. Cancer* **2013**, *133*, 2398–2407.
35. Ding, H.; Inoue, S.; Ljubimov, A. V.; Patil, R.; Portilla-Arias, J.; Hu, J.; Konda, B.; Wawrowsky, K. A.; Fujita, M.; Karabalin, N.; *et al*. Inhibition of Brain Tumor Growth by Intravenous Poly (β-L-Malic Acid) Nanobioconjugate with pH-Dependent Drug Release. *Proc. Natl. Acad. Sci. U.S.A.* **2010**, *107*, 18143–18148.
36. Langer, R.; Weissleder, R. Nanotechnology. *JAMA* **2015**, *313*, 135–136.
37. Choi, B. D.; Kuan, C. T.; Cai, M.; Archer, G. E.; Mitchell, D. A.; Gedeon, P. C.; Sanchez-Perez, L.; Pastan, I.; Bigner, D. D.; Sampson, J. H. Systemic Administration of a Bispecific Antibody Targeting EGFRvIII Successfully Treats Intracerebral Glioma. *Proc. Natl. Acad. Sci. U.S.A.* **2013**, *110*, 270–275.
38. Fitzgerald, D. P.; Subramanian, P.; Deshpande, M.; Graves, C.; Gordon, I.; Qian, Y. Z.; Snitkovsky, Y.; Liewehr, D. J.; Steinberg, S. M.; Paltán-Ortiz, J. D.; *et al*. Opposing Effects of Pigment Epithelium-Derived Factor on Breast Cancer Cell *versus* Neuronal Survival: Implication for Brain Metastasis and Metastasis-Induced Brain Damage. *Cancer Res.* **2012**, *72*, 144–153.
39. Kominsky, S. L.; Tyler, B.; Sosnowski, J.; Brady, K.; Doucet, M.; Nell, D.; Smedley, J. G., 3rd; McClane, B.; Brem, H.; Sukumar, S. Clostridium Perfringens Enterotoxin as a Novel-Targeted Therapeutic for Brain Metastasis. *Cancer Res.* **2007**, *67*, 7977–7982.
40. Kong, D. S.; Kim, M. H.; Jeon, J. W.; Kim, S. Y.; Kim, M. S.; Joo, K. M.; Park, K.; Nam, D. H. Antitumor Activity of ZD6474 in a Metastatic Orthotopic Brain Tumor Model. *Mol. Med. Rep.* **2008**, *1*, 343–346.
41. Valiente, M.; Obenauf, A. C.; Jin, X.; Chen, Q.; Zhang, X. H.; Lee, D. J.; Chaft, J. E.; Kris, M. G.; Huse, J. T.; Brogi, E.; *et al*. Serpins Promote Cancer Cell Survival and Vascular Co-Option in Brain Metastasis. *Cell* **2014**, *156*, 1002–1016.
42. Fujita, M.; Lee, B. S.; Khazenzon, N. M.; Penichet, M. L.; Wawrowsky, K. A.; Patil, R.; Ding, H.; Holler, E.; Black, K. L.; Ljubimova, J. Y. Brain Tumor Tandem Targeting Using a Combination of Monoclonal Antibodies Attached to Biopoly(β-L-Malic Acid). *J. Controlled Release* **2007**, *122*, 356–363.
43. Bien-Ly, N.; Yu, Y. J.; Bumbaca, D.; Elstrott, J.; Boswell, C. A.; Zhang, Y.; Luk, W.; Lu, Y.; Dennis, M. S.; Weimer, R. M.; *et al*. Transferrin Receptor (TfR) Trafficking Determines Brain Uptake of TfR Antibody Affinity Variants. *J. Exp. Med.* **2014**, *211*, 233–244.

44. Gaviani, P.; Silvani, A.; Lamperti, E.; Botturi, A.; Simonetti, G.; Ferrari, D.; Salmaggi, A. Neuro-Oncological Diagnosis in Patients without Histological Confirmation. *Neurol. Sci.* **2011**, *32* (Suppl 2), S213–215.
45. Hatake, K.; Tokudome, N.; Ito, Y. Next Generation Molecular Targeted Agents for Breast Cancer: Focus on EGFR and VEGFR Pathways. *Breast Cancer* **2007**, *14*, 132–149.
46. Peddi, P. F.; Hurvitz, S. A. PI3K Pathway Inhibitors for the Treatment of Brain Metastases with a Focus on HER2+ Breast Cancer. *J. Neurooncol.* **2014**, *117*, 7–13.
47. Nair, R.; Roden, D. L.; Teo, W. S.; McFarland, A.; Junankar, S.; Ye, S.; Nguyen, A.; Yang, J.; Nikolic, I.; Hui, M.; Morey, A.; *et al*. C-Myc and Her2 Cooperate to Drive a Stem-Like Phenotype with Poor Prognosis in Breast Cancer. *Oncogene* **2013**, *33*, 3992–4002.
48. Singh, S.; Chellappan, S. Lung Cancer Stem Cells: Molecular Features and Therapeutic Targets. *Mol. Aspects Med.* **2014**, *39*, 50–60.
49. Rosen, J. M.; Jordan, C. T. The Increasing Complexity of the Cancer Stem Cell Paradigm. *Science* **2009**, *324*, 1670–1673.
50. Fritz, A.; Sinha, S.; Marella, N.; Berezney, R. Alterations in Replication Timing of Cancer-Related Genes in Malignant Human Breast Cancer Cells. *J. Cell Biochem.* **2013**, *114*, 1074–1083.
51. Ljubimova, J. Y.; Ding, H.; Portilla-Arias, J.; Patil, R.; Gangalum, P. R.; Chesnokova, A.; Inoue, S.; Rekechenetskiy, A.; Nassoura, T.; Black, K. L.; *et al*. Polymalic Acid-Based Nano Biopolymers for Targeting of Multiple Tumor Markers: An Opportunity for Personalized Medicine? *J. Vis. Exp.* **2014**, *88*, e50668.
52. Barge, A.; Cravotto, G.; Gianolio, E.; Fedeli, F. How to Determine Free Gd and Free Ligand in Solution of Gd Chelates. A Technical Note. *Contrast Media Mol. Imaging* **2006**, *1*, 184–188.
53. Nag, A.; Mitra, G.; Ghosh, P. C. A Colorimetric Assay for Estimation of Polyethylene Glycol and Polyethylene Glycolated Protein Using Ammonium Ferrothiocyanate. *Anal. Biochem.* **1996**, *237*, 224–231.
54. Carlsson, J.; Drevin, H.; Axen, R. Protein Thiolation and Reversible Protein-Protein Conjugation. N-Succinimidyl 3-(2-Pyridyldithio)Propionate, a New Heterobifunctional Reagent. *Biochem. J.* **1978**, *173*, 723–737.